Light Metals 2007 *Edited by Morten Sorlie* ***TMS (The Minerals, Metals & Materials Society), 2007***

MODELING THE EFFECT OF THE ANODE CHANGE SEQUENCE WITH A NON-LINEAR SHALLOW WATER STABILITY MODEL

Vanderlei Gusberti[1], Dagoberto S. Severo[2], André F. Schneider[2], Elton C. V. Pinto[2], Antônio C. F. Vilela[1].

[1] LASID – PPGEM – Programa de Pós Graduação em Engenharia Metalúrgica, Minas e Materiais, Av. Bento Gonçalves, 9500 Porto Alegre - RS - Brazil
[2] PCE Engenharia S/S Ltda, Rua Caete 162, Porto Alegre - RS - Brazil

Keywords: Aluminum reduction, Magnetohydrodynamics, Interface stability, Shallow water, Anode change sequence

Abstract

Numerical simulation of the magnetohydrodynamic (MHD) stability of the aluminum electrolysis cells has become an important tool for improving its design and operation efficiency. This paper presents a non-linear transient shallow water stability model and its application to the study on the stability of an existent cell. In the model, current density in the liquid metal pad, magnetic field generated by the currents inside the cell and subsequently, metal-bath interface wave shape are calculated at each time step.

Anode changing greatly disturbs cell stability. During the anode change sequence, large current density disturbances occur, which produce a different MHD stability pattern after each anode change. We use the model to investigate the effect of different anode change patterns on MHD stability of the metal-bath interface. With the predictions of the model, it was possible to develop a new anode change sequence that improves cell stability.

Introduction

For more than a century, primary aluminum is obtained by a complex process of electrochemical reduction of alumina in Hall-Héroult cells. Usually, many cells are connected in series to form a pot line. In a smelter there can be one or more pot lines. A large amount of DC current in a pot line flows from cell to cell in aluminum busbars. Inside each cell, current flows downwards through the anodes, bath, molten metal pad and cathode carbon block. Steel collector bars take the current laterally out from the cathode blocks to the busbars.

The core of a reduction cell is the liquid bath and metal region. The bath is slightly lighter and floats on top of the metal creating a two-phase system of immiscible liquids. Gravity only would keep the metal-bath interface flat and horizontal. However, in an operating cell, the combination of the electric current and the magnetic field gives volumetric forces, known as Lorentz or electromagnetic forces. These set the metal and the bath in motion and deform the metal-bath interface. The deformation of the interface perturbs the electric field in the liquids and subsequently the Lorentz forces, thus creating a self-exciting mechanism of bath-metal interface waves described by many authors [1-12]. This behavior is widely known in the aluminum industry as “metal pad roll”. Typically, metal pad roll presents interfacial waves with period of 20 - 60 s. The schematic drawing of the Figure 1 shows an interface wave in the cell and its influence on the electric current distribution in the bath and the metal pad. The bath is far more resistive than the metal and the anodes. This makes the current density in the bath nearly vertical and much greater at the wave crest than at the trough. The current lines change the direction at the bath-metal interface and the current is redistributed horizontally in the metal pad.

Magnetohydrodynamics (MHD) is the science that studies the interactions between electromagnetic forces and fluid flow. This paper presents the development and an application of transient non-linear shallow water MHD instability model of aluminum electrolysis cells and its application on the study of anode change sequences.

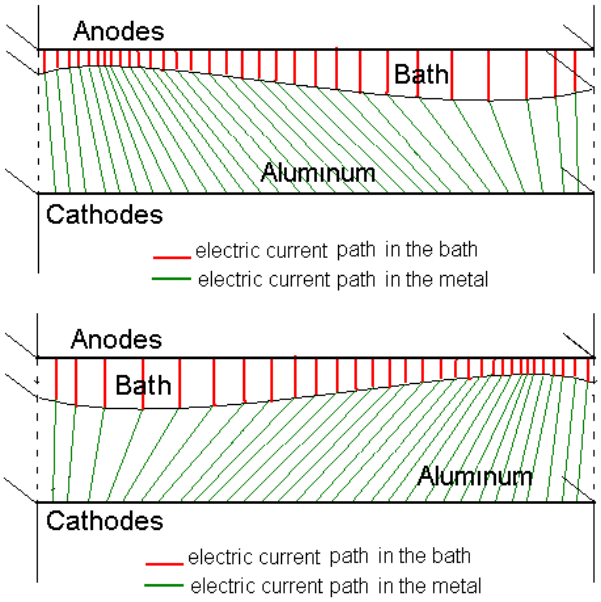

Figure 1. Interface perturbations and their influence on the electric current distribution.

The bath layer is the most resistive part of the electric path. The resistive generation of heat in the bath layer is proportional to the anode-to-cathode distance (ACD), therefore, this layer should be as thin as possible. However, the interface waves may appear at small ACD and make the cell resistance unstable. This promotes the mass transfer of liquid aluminum to the bath and to the gas layer near the anodes and decreases current efficiency. The minimum ACD at which the cell remains stable depends on cell design, busbar design and cell operation. Cell amperage also plays a major role since the electromagnetic forces in the liquid zone increase proportionally to the square of the current.

Amperage increase has limits, largely determined by the MHD and heat balance of the cell. Thorough understanding and control of cell MHD instability are key to high current and energy efficiency.

In 1976 Urata et al [1] characterized the instability mechanism for the first time. Since then, many models with different approaches have been published in order to predict MHD instabilities. With the help of these models it was possible to increase cell currents and efficiency in many cases. In general, these models can be classified in two types: linear perturbation analysis of waves [1-6] and transient MHD analysis [7-11]. The latter uses transient shallow-water [7-9] or three-dimensional models [10-11]. In these models, cell stability is inferred from the decreasing or increasing wave amplitudes with time.

In the present work, a transient shallow water model is used. It is less computationally intensive than the 3D models and includes more detailed physics than the linear perturbation analysis. Our goal is to develop a fast algorithm, so that many tests can be done in a short period of time. Nevertheless our algorithm includes the main non-linearity present in the MHD waves in cells as well as the electric current distribution. This is particularly important in the study of aggressive cell disturbances, such as anode changing, cathode sludge and bad ledge shape due to poor heat balance.

The steady magnetic field is calculated separately using the commercial code ANSYS and enters in the model as an input. The transient electric model comprises the anode ring busbar, anode rods, anodes, bath and liquid metal pad. The anode ring busbar and the metal pad are assumed to be equipotentials. The model calculates the electric potential from Poisson equation at each time step. Therefore, large amplitude waves can be studied. At each time step, the transient model calculates also the magnetic field perturbation arising from the perturbed currents using Biot-Savart law. With the new distribution of electric currents, magnetic fields and electromagnetic forces, the new wave shape is computed from the wave equation which is derived from shallow water theory.

Using this methodology, many situations and their influence on the cell stability can be studied, such as: anode change, different ledge profiles, channel width, ACD variation, metal level variation, line current variation, cathode sludge and busbar retrofit.

In this work we used the model to study several options of anode change sequences in the EPT14 cell at TRIMET ALUMINIUM AG located in Essen (Germany). During the anode change sequence, anodes with different ages carry different currents due to local variations of anode resistance, metal pad height and frozen ledge. The position of the new and old anodes affects the current density in the metal, modifying the patterns of forces and interface deformation. It is possible to identify critical anode positions in the change sequence at which the stability is more disturbed. The 3 sequences already used by the smelter were tested and, with help of the stability model, a new one is proposed. The model has an empirical curve of anode current with respect to anode age, given to PCE by the smelter staff.

Model Description

Geometry

The two layers of liquids are discretized in the horizontal plane where the variables are calculated numerically. No vertical meshing is needed for the shallow water approach. Anodes and anode rods are represented individually in the electric circuit as extra resistances before the current enters into the bath.

Model Inputs

The steady state magnetic field is obtained by a 3D Finite Element Model using the commercial software package ANSYS. All relevant aspects of the cell are taken into account, such as external conductors (busbar arrangement), internal conductors (liquid layers, collector bars, anodes and cathodes), and the steel shell. In ANSYS, the electromagnetic calculations are done with flat bath-metal interface. The steady state distribution of current density at the cathode block - liquid metal interface is also supplied by the ANSYS calculation. The details of the implementation in ANSYS are found in [13].

Electric Potential

In the stability model, the electric potential V is calculated as a primary variable from the Laplace Equation (1) in each time step using standard Finite Volume Method,

$$\nabla \cdot (\sigma \nabla V) = 0 \tag{1}$$

where σ is electrical conductivity for the respective material. The current density $\mathbf{J}$ in each material is calculated from Equation (2):

$$\mathbf{J} = -\sigma \nabla V \tag{2}$$

The electric model boundary conditions are: reference potential equal to zero at the anodic busbar ring and the current density calculated by the ANSYS model at the top of the cathode block. The calculated current density is separated into the steady part $\mathbf{J_0}$ (calculated by ANSYS with flat interface) and the transient part $\mathbf{j}$ that is due to the interface distortion:

$$\mathbf{J} = \mathbf{J_0} + \mathbf{j} \tag{3}$$

At this point, it is convenient to define total quantities as capital characters, perturbed quantities as small characters and steady quantities as capital characters with the subscript "**0**".

Magnetic Flux Density

Since the steady state magnetic flux density $\mathbf{B_0}$ is given as input to the present model, only the perturbed magnetic flux density is calculated at each time step from the Biot-Savart law:

$$\mathbf{b} = \frac{\mu_0}{4\pi} \iiint_{volC} \frac{\mathbf{j} \times \mathbf{r}}{\mathbf{r}^3} d(volC) \tag{4}$$

where: $\mathbf{b}$ is the transient part of the magnetic flux density, μ_0 is the magnetic permeability of vacuum, $volC$ is the volume of the conductor and $\mathbf{r}$ is the distance vector between the conductor and the point of interest.

Shallow Water and Wave Equation

The simplification of the Navier-Stokes equation, the so called Shallow Water equation, was developed for situations when the height of the liquid layer is small in comparison with the other

dimensions of the liquid cavity, which is the case for the aluminum cell. The simplification is valid in the absence of breaking waves.

The Shallow Water equation for a single liquid layer (5) and the continuity equation (6) have the form:

$$\rho\left(\frac{\partial \mathbf{V}}{\partial t}+\mathbf{V}\bullet\nabla\mathbf{V}\right)+\rho g\nabla H=-\nabla P+\mu_{eff}\left(\nabla^2\mathbf{V}\right)+\mathbf{F}_{EM} \quad (5)$$

$$\nabla\bullet(H\mathbf{V})=-\frac{\partial H}{\partial t} \quad (6)$$

where: $\mathbf{V}$ is the velocity vector, ρ is the fluid density, g is the vertical gravity component, H is the height of the fluid layer, P is the pressure, μ_{eff} is effective dynamic viscosity and $\mathbf{F}_{EM}$ is electromagnetic force.

The variables from equations (5) and (6) are decomposed in steady and transient part resulting in a set of averaged steady equations and a set of perturbed variables equations. Our attention is focused on the perturbed problem:

$$\rho\left(\frac{\partial \mathbf{v}}{\partial t}+\mathbf{V}_0\bullet\nabla\mathbf{v}+\mathbf{v}\bullet\nabla\mathbf{V}_0+\mathbf{v}\bullet\nabla\mathbf{v}\right)+\rho g\nabla h=-\nabla p+\mu_{eff}\nabla^2\mathbf{v}+\mathbf{f} \quad (7)$$

$$\nabla\bullet(H_0\mathbf{v}+h\mathbf{V}_0+h\mathbf{v})=-\frac{\partial h}{\partial t} \quad (8)$$

Some simplifications presented in earlier works are adopted:

- The velocity perturbations are small, the second order term $\mathbf{v}\bullet\nabla\mathbf{v}$ can be neglected.
- The influence of the background flow on the stability is negligible in comparison to Lorentz force perturbations, $\mathbf{V}_0=0$. In fact, Sun et al [8] showed that very different background flows can influence the growth of waves by a few percent, but considering comparisons in a similar situation with the same geometry this effect should be negligible.
- The fluid is inviscid. The waves are not damped by friction, $\mu_{eff}=0$.
- The bath current density is purely vertical due to its high resistivity. $\mathbf{J}_b=(0,0,J_{bz})$.

The equations (7) and (8) are reorganized and in a new set of equations for each fluid layer (subscript "a" stands for aluminum and "b" for bath).
For the aluminum layer:

$$\rho_a\frac{\partial \mathbf{v}_a}{\partial t}+\rho_a g\nabla\eta=-\nabla p+\mathbf{f}_a \quad (9)$$

$$H_a(\nabla\bullet\mathbf{v}_a)=-\frac{\partial\eta}{\partial t} \quad (10)$$

For the bath layer:

$$\rho_b\frac{\partial \mathbf{v}_b}{\partial t}+\rho_b g\nabla\eta=-\nabla p+\mathbf{f}_b \quad (11)$$

$$H_b(\nabla\bullet\mathbf{v}_b)=\frac{\partial\eta}{\partial t} \quad (12)$$

At the interface, the two liquids have the same pressure ($p_a = p_b = p$). In the cavity, an increase of the aluminum layer decreases the bath layer in the same position by the same magnitude: $h_a = -h_b = \eta$, that represents the vertical interface displacement.

Applying the divergence operator on the momentum equations (9) and (11), and substituting (10) and (12), we have:

$$-\frac{\rho_a}{H_a}\frac{\partial^2\eta}{\partial t^2}+\rho_a g\nabla^2\eta=-\nabla^2 p+\nabla\bullet\mathbf{f}_a \quad (13)$$

$$\frac{\rho_b}{H_b}\frac{\partial^2\eta}{\partial t^2}+\rho_b g\nabla^2\eta=-\nabla^2 p+\nabla\bullet\mathbf{f}_b \quad (14)$$

Now we subtract equation (13) from equation (14) to obtain a single wave equation:

$$\left(\frac{\rho_a}{H_a}+\frac{\rho_b}{H_b}\right)\frac{\partial^2\eta}{\partial t^2}-\left(\rho_a-\rho_b\right)g\nabla^2\eta=-\nabla\bullet\left(\mathbf{f}_a-\mathbf{f}_b\right) \quad (15)$$

With boundary condition at the sidewalls:

$$\left(-\left(\rho_a-\rho_b\right)g\nabla\eta+\left(\mathbf{f}_a-\mathbf{f}_b\right)\right)\bullet\mathbf{n}=0 \quad (16)$$

where $\mathbf{n}$ is the normal vector pointing to the lateral boundary.
The wave equation (15) becomes the same used in earlier works and the boundary condition (16) is the same proposed by Droste et al [2]. However, for the calculation of the source term on the right hand side of Equation (15) we use a more general approach for perturbed current density calculation and we include also the perturbed magnetic field. The equation (15) tracks the wave evolution. It is quickly solved in a marching algorithm. At this point, we focus on the electromagnetic source term: $-\nabla\bullet\left(\mathbf{f}_a-\mathbf{f}_b\right)$. The expression for the total Lorentz force can be decomposed:

$$\mathbf{F}_0+\mathbf{f}=\left(\mathbf{J}_0+\mathbf{j}\right)\times\left(\mathbf{B}_0+\mathbf{b}\right) \quad (17)$$

Eliminating the stationary part:

$$\mathbf{f}=\left(\mathbf{J}_0\times\mathbf{b}\right)+\left(\mathbf{j}\times\mathbf{B}_0\right)+\left(\mathbf{j}\times\mathbf{b}\right)=\left(\mathbf{J}\times\mathbf{b}\right)+\left(\mathbf{j}\times\mathbf{B}_0\right) \quad (18)$$

At the interface, the vertical current density is equal in the bath and in the metal (Figure 1) and so is the horizontal magnetic field generated by it. Perturbed magnetic fields due to horizontal currents in the metal are vertical only in the metal and horizontal only in the bath. The perturbed forces for metal and bath are then:

$$\mathbf{f}_a=\begin{pmatrix} j_{ay}B_{0z}-j_zB_{0y}+J_{ay}b_z-J_zb_{y\perp} \\ j_zB_{0x}-j_{ax}B_{0z}+J_zb_{x\perp}-J_{ax}b_z \end{pmatrix} \quad (19)$$

$$\mathbf{f}_b=\begin{pmatrix} -j_zB_{0y}-J_zb_{y\perp}-J_zb_{y\perp} \\ j_zB_{0x}+J_zb_{x\perp}+J_zb_{x\perp} \end{pmatrix} \quad (20)$$

Where $bx_{\perp}$, $by_{\perp}$ are the perturbed horizontal magnetic fields generated by the floating vertical current, bz is the perturbed horizontal field in the metal, generated by the horizontal current in the metal, and $bx_{\parallel}$, $by_{\parallel}$ are the perturbed horizontal magnetic fields, in the bath layer, generated by horizontal current perturbations in the metal pad.

After some cancellations, the divergence of the source is obtained and, finally, the wave equation solved by the algorithm is:

$$\left(\frac{\rho_a}{H_a}+\frac{\rho_b}{H_b}\right)\frac{\partial^2\eta}{\partial t^2}-(\rho_a-\rho_b)\,g\left(\frac{\partial^2\eta}{\partial x^2}+\frac{\partial^2\eta}{\partial y^2}\right)= -\frac{\partial\left(j_y B_{0z}+J_y b_z+J_z b_{y\perp}\right)}{\partial x}-\frac{\partial\left(-j_x B_{0z}-J_x b_z-J_z b_{x\perp}\right)}{\partial y} \quad (21)$$

Stability Criterion

The stability criterion adopted is the rate of increase of the wave amplitude. An integration of the wave displacement is done at each time step, and then the growth rate of the total displacement in [1/s] is calculated.

Case Study: EPT14 at TRIMET ALUMINIUM AG

With collaboration of TRIMET ALUMINIUM AG, we performed a complete MHD study on the EPT14 cell. The pot is end-to-end, magnetically compensated, and operates at 160 kA. Figure 2 shows the three magnetic flux density components obtained by the detailed ANSYS model.

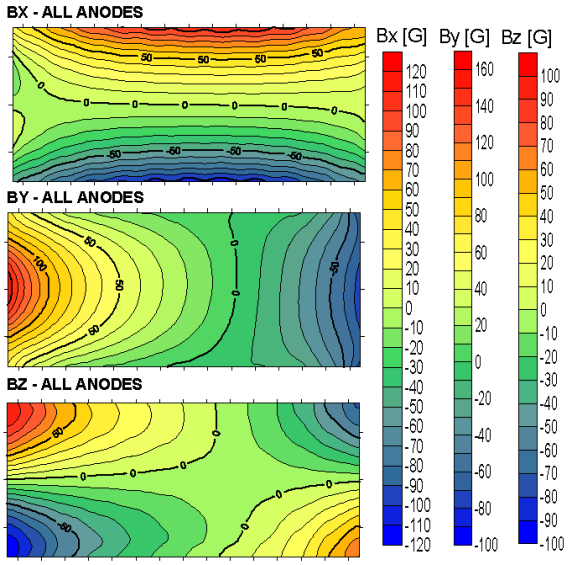

Figure 2: Bx (horizontal longitudinal), By (horizontal transversal) and Bz (vertical) magnetic flux densities [G], all anodes carrying the same current.

The wave evolution was calculated with the transient stability model. Starting from a small perturbation (a sum of many basic modes), the wave develops and increases its amplitude depending on the MHD self-exciting mechanism. The resulting wave shape can be different for each given electromagnetic situation. The type of the initial perturbation does not influence the final developed wave shape according to our tests. Figure 3 presents the wave evolution for the basic case with all anodes carrying the same current. The growth rate of the wave found for this case is 0.0138 1/s.

Anode Change Sequences

Three sequences already tested in the plant were calculated: Rota 1, Rota 2 and Rota 3 [14]. A new sequence, based on the calculations is proposed: Rota 4. There are 26 anodes in the cell, in most changes a pair of anodes is changed simultaneously. Because of the uneven number of anodes at each side of the cell, a single anode change occasionally occurs. The sequences are described in Figures 4 to 7.

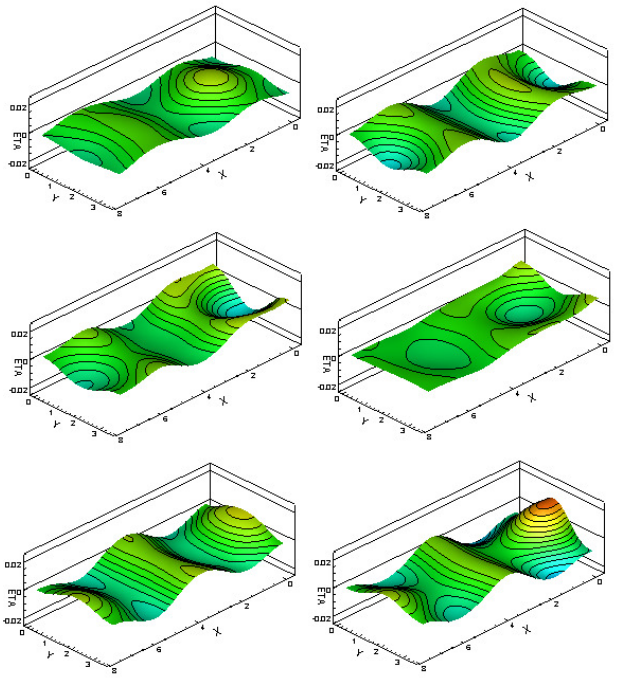

Figure 3: Wave calculated by the transient stability model (model with all anodes carrying the same current)

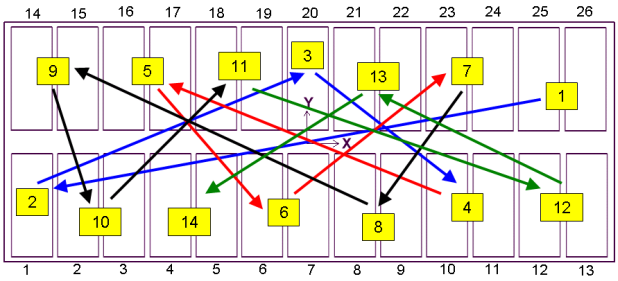

Figure 4: Anode change sequence (Rota 1)

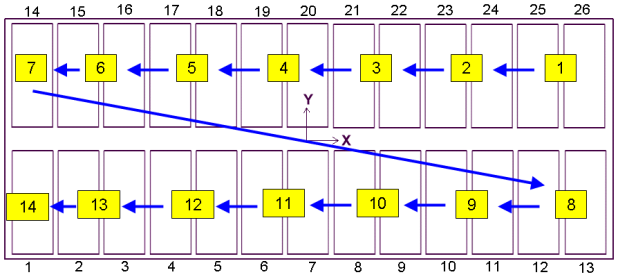

Figure 5: Anode change sequence (Rota 2)

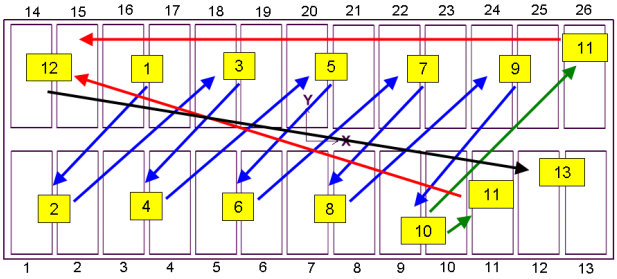

Figure 6: Anode change sequence (Rota 3)

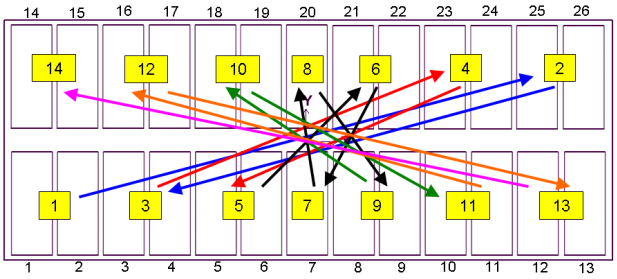

Figure 7: Anode change sequence (Rota 4)

Repeating the calculation process (steady magnetics and transient MHD instability) for each anode change, the growth rate in all situations was obtained. These results are shown in Figure 8.

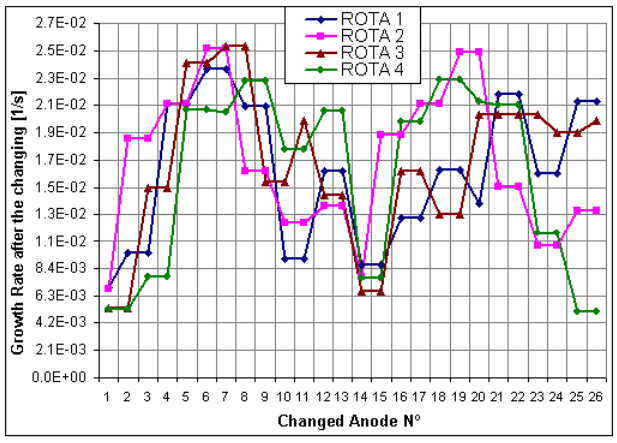

Figure 8: Calculated wave growth rate after each anode change

It is possible to identify a critical region in the pot, a change of anodes 5 to 8 produces higher instability levels for all patterns. Objective for developing Rota 4 was to achieve a reduced overall wave growth rate, with a decreasing number of critical anode change positions. Furthermore it was intended to keep the anode change sequence easy regarding pot tending. The combination of these objectives were achieved in a sequence where the next anode is always changed in the diagonal opposite quarter of the pot as shown in Figure 7 (inverted sequential pattern). In this way the horizontal current component in the metal pad is equalized.

The average growth rate for each Rota is presented in Figure 9, compared with the "ideal situation" when all anodes carry the same current (which is never the case in a real cell).

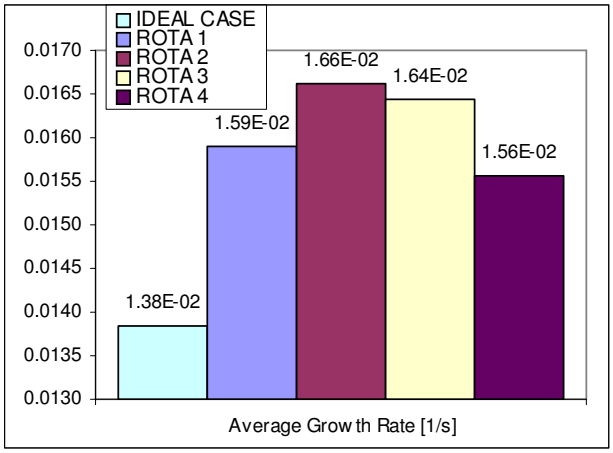

Figure 9: Average growth rate for each Rota (1,2,3 and 4) and the "ideal case" with all anodes carrying the average current

New sequences can be proposed and we believe that it is possible to achieve even better instability results. Other factors should be taken into account such as thermal behavior and operational issues in order to decide which anode change sequence should be adopted to achieve optimal performance results.

Results Obtained by the Smelter

The three anode change rotas 1, 2 and 3 were trialed at the TRIMET smelter in Essen for a period of 6 months in potline 2. Rota 1 comprised 40 pots, rota 2 consisted of 12 pots and rota 3 was applied to 20 pots. The detailed results of these tests can be found in [14], while the current efficiencies are displayed in Figure 10.

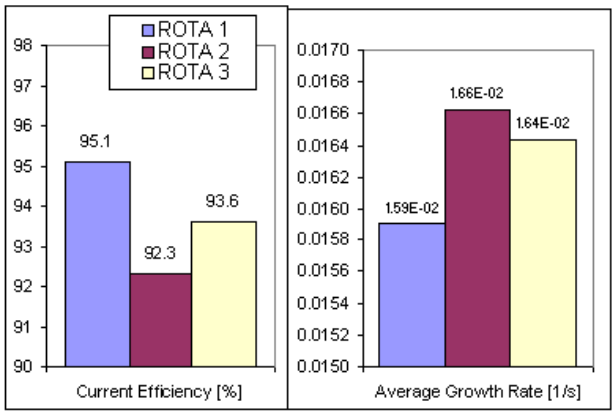

Figure 10: Current efficiency achieved during the test for each Rota (left), calculated average growth rate after anode changes

The results show a consistent inverse correlation between the growth rate of waves and the current efficiency observed in practice. It is known [1] that surface waves induce the jumping of particles of surface metal to bath and the localized ACD squeezing, both processes promoting aluminum re-oxidation and consequently current efficiency loss.

Although thermal calculation was not included in the present work, an important thermal phenomenon was considered: the measured pick up of current in a new anode, used to estimate the anode resistance curve, which is influenced by the thermal condition of the new anode and its neighbors.

Conclusion

A transient non-linear shallow water stability model was successfully developed. The influence on the cell stability of many phenomena can be studied, such as: anode change, different ledge profiles, channel width, ACD variation, metal level variation, line current variation, cathode sludge and busbar retrofit.

In this paper, the model was applied to the comparison of anode change sequences. Valuable information on which changed anodes affect the stability most was obtained.

Three different change sequences were tested in EPT14 pots during 6 months. The current efficiencies for the three anode change patterns achieved in real cells are in excellent agreement with the model instability predictions and the waves growth rates.

With the understanding provided by the model, it was possible to propose a new anode change sequence which decreased the highest peaks of instability, as well as decreased the average growth rate for the whole anode change sequence.

Acknowledgement

The authors wish to thank the TRIMET ALUMINIUM AG, in special, Mr. Martin Iffert for his suggestions and collaboration with technical data and test results. Many thanks are also to Mr. Vinko Potocnik for his critical and careful review of the manuscript.

References

1. N. Urata, K. Mori and H. Ikeuchi, “Behavior of bath and molten metal in aluminium electrolitic cell”, *Kaikinzoku (Light Metals, Japan)*, 26, (1976), 573-583.

2. Ch. Droste, M. Segatz and D. Vogelsang, “Improved 2-Dimensional Model for Magnetohydrodynamic Stability Analysis in Reduction Cells”, *Light Metals* (1998), 419-428.

3. J. Antille, J. Descloux, M. Flueck and M. V. Romerio, “Eigenmodes and Interface Description in a Hall-Heroult Cell,” *Light Metals*, (1999), 333-338.

4. A. D. Sneyd, “Interfacial Instabilities in Aluminium Reduction Cells,” *Journal of Fluid Mechanics*, 236 (1992), 111-126.

5. P. A. Davidson and R. I. Lindsay, “Stability of Interfacial Waves in Aluminium Reduction Cells,” *Journal of Fluid Mechanics*, 362 (1998), 273-295.

6. M. F. El-Demerdash, S. M. El-Raghy and Z. Bassuny, “Estimation of Aluminium Cell Stability for a given Bus-bar Design,” *Light Metals*, (1995), 289-294.

7. O. Zikanov, H. Sun and D. P. Ziegler, “Shallow Water Model of Flows in Hall-Héroult Cells,” *Light Metals*, (2004), 445-451.

8. H. Sun, B. A. Finlayson O. Zikanov, and D. P. Ziegler, “The Influence of the Basic Flow and Interface Deformation on Stability of Hall-Héroult Cells,” *Light Metals*, (2005), 437-441.

9. L. Leboucher, K. Pericleous, I. Panaitescu and M. Repetto, “A Finite-Volume Shallow Layer Method, for the MHD Instabilities in an Aluminium Production Cell”, *Second International Conference on CFD in Minerals and Process Industries (Australia)*, 1999, 335-338.

10. M. Segatz, D. Vogelsang, Ch. Droste and P. Baekler, “Modeling of Transient Magneto-Hydrodynamic Phenomena in Hall-Héroult Cells”, *Light Metals*, (1993), 361-368.

11. V. Potocnik, “Modeling of Metal-Bath Interface Waves in Hall-Heroult Cells Using ESTER/PHOENICS,” *Light Metals*, (1989), 227-235.

12. V. Bojarevics and M. V. Romerio, “Long waves instability of liquid metal-electrolyte interface in. aluminum electrolysis cells: a generalization of Sele’s criterion*”, Eur. J. Mech., B/Fluids, 13*, (1994), pp. 33-56.

13. D. S. Severo, A. F. Schneider, E. C. V. Pinto, V. Gusberti and V. Potocnik, “Modeling Magnetohydrodynamics Of Aluminum Electrolysis Cells With ANSYS And CFX”, *Light Metals*, (2005), 475-480.

14. M. Iffert, M. Skyllas-Kazacos and B. Welch, “Challenges in Mass Balance Control”, *Light Metals*, (2005), 385-391.